Hawlader, B. C., Muhunthan, B. & Imai, G. (2008). *Géotechnique* **58**, No. 2, 133–141 [**doi:** 10.1680/geot.2008.58.2.133]

State-dependent constitutive model and numerical solution of self-weight consolidation

B. C. HAWLADER*, B. MUHUNTHAN† and G. IMAI‡

A new constitutive model is developed for the compressibility behaviour of soft clay sediments at low effective stress level. Central to this model is the realisation that at low effective stress levels the void ratio–effective stress paths of soil elements are non-unique, and dependent very much on their state. Beyond a threshold stress level, these relationships become unique. These observations have been used to develop a state-dependent constitutive model for the compressibility behaviour of soft sediments. Methods to obtain the input parameters of the model are discussed. The proposed model is used to solve finite-strain one-dimensional consolidation with pertinent initial and boundary conditions. The analyses performed using a finite difference computer code predict better the observed phenomena associated with self-weight consolidation, especially during its early stages. The comparison of the predictions shows that the present model can capture the decrease in void ratio patterns, as observed in experiments at low effective stresses, and which cannot be modelled using existing constitutive relationships.

KEYWORDS: clays; compressibility; consolidation; numerical modelling; sedimentation

Un nouveau modèle constitutif du comportement de la compressibilité de sédiments d'argile molle sous l'effet de faibles tensions efficaces est développé. Le principe fondamental de ce modèle est la prise de conscience du fait qu'en présence de faibles tensions efficaces, les chemins de l'indice de vide/des tensions efficaces des éléments du sol ne sont pas uniques et sont, dans une grande mesure, tributaires de leur état. Au-delà d'un seuil de tension, ces rapports deviennent uniques. Ces observations ont été utilisées pour créer un modèle constitutif lié à l'état du comportement de compressibilité de sédiments meubles. On discute de méthodes utilisées pour obtenir les paramètres d'entrée du modèle, et le modèle proposé est utilisé pour résoudre une consolidation monodimensionnelle à déformation finie, comportant des conditions initiales et limites pertinentes. Les analyses effectuées en appliquant un code informatique à différence finie permettent de mieux prédire les phénomènes observés relativement à la consolidation à poids propres, en particulier dans les phases initiales. La comparaison entre les prédictions indique que le présent modèle est en mesure de saisir la réduction des tendances des indices de vide, relevée au cours d'expériences en présence de faibles tensions efficaces, et ne pouvant pas être modélisée en utilisant des rapports constitutifs existants.

INTRODUCTION

The genesis of developing soil deposits from a thin slurry or suspension consists of three stages, as shown in Fig. 1 (Imai, 1981). Flocs generate in the flocculation stage, but no settling takes place. In the settling stage the flocs gradually settle and form a layer of sediment, which undergoes consolidation and reduction of void ratio with time. The boundary between the upper settling zone and the sediment is the birthplace of new sediment. The thickness of the settling zone gradually decreases with time and eventually reduces to zero, leaving the sediment thus formed to undergo self-weight consolidation in the consolidation stage. Initiation of consolidation occurs only when a continuous soil structure is formed within the sediment. The density at which the soil structure is formed has been referred to as 'structural density' (Sills, 1995). If the initial density of the slurry is larger than the structural density, soil structure could exist from the beginning, and self-weight consolidation initiates from the start of the test.

The mathematical model describing the process of densification of slurry involves the settling of solid particles in suspension and the consolidation of the sedimented layer. The consolidation behaviour of sediment is an extremely complex problem, which encompasses the development of mathematical models, laboratory testing, associated interpretations, identification of material parameters, and engineering judgement. Several mathematical models have been developed in the past to describe sedimentation in a suspension, and self-weight consolidation of the resulting deposit. The non-linear finite-strain consolidation theory (Gibson *et al.*, 1981) is generally considered the state of the art for predict-

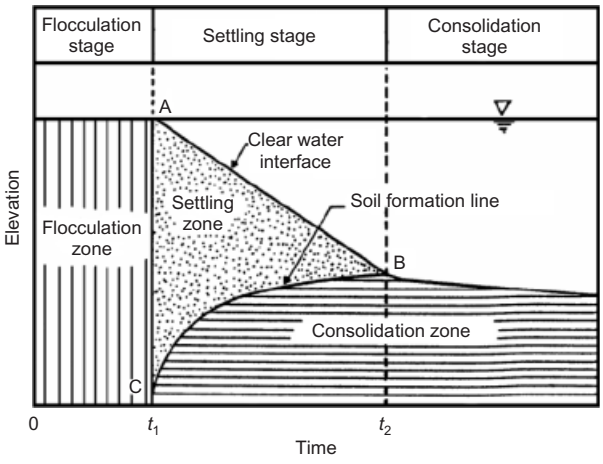

Fig. 1. General characteristics of sedimentation and self-weight consolidation (Imai, 1981)

Manuscript received 2 November 2005; revised manuscript accepted 9 October 2007.
Discussion on this paper closes on 1 September 2008, for further details see p. ii.
* AMEC Earth and Environmental, Calgary, Alberta, Canada.
† Department of Civil and Environmental Engineering, Washington State University, Pullman, USA.
‡ Deceased; formerly Department of Civil Engineering, Yokohama National University, Japan.

ing self-weight consolidation in engineering applications. Toorman (1996) has shown that although many different approaches and their resultant models have their own history, and originated in different fields of natural sciences, they can all be described under a unified theory. It was further shown that the resulting unified mathematical model was consistent with the chemical and geotechnical approaches and in particular with Gibson's formulation. However, the success of the prediction of self-weight consolidation behaviour using mathematical models is critically dependent on the choice of an appropriate constitutive model.

Sidere, a seminar held in Oxford in 2000, consisted of 'Class A' prediction of the behaviour of a suite of self-weight consolidation experiments conducted at the University of Oxford on sediment (LL = 39%, PL = 28% and G_s = 2·72) from the River Schelde in Antwerpen, Belgium (Bartholomeeusen *et al*., 2002). The participants were provided with the data of four settling column experiments to establish material properties. They were then requested to predict the fifth experiment. The numerical predictions by different researchers consistently showed a pattern of a very fast settlement during the initial stages of consolidation, with a significant portion of the predicted settlement occurring within two days. By contrast, the experimental results showed substantially lower settlement during this period. In fact, some of the predicted settlements were as high as 300% of the observed settlement at the end of two days. Based on a critical evaluation of the relationships used in the models, it was concluded that failure to account properly for the compressibility behaviour of soil at the low effective stress level had contributed in large measure to the differing predictions.

This paper presents a detailed examination of the compressibility behaviour of soft soils in the low effective stress region. It is shown that the void ratio–effective stress relationships of soil elements in a settling column are not unique at these stress levels, and that their form becomes unique only beyond a threshold stress. A constitutive formulation that captures this distinct behaviour is proposed. The governing equation of consolidation is solved, with the proposed constitutive formulation and appropriate initial and boundary conditions, using a finite difference method. The numerical code has been used to re-analyse the Sidere test results.

MATHEMATICAL DESCRIPTION OF SELF-WEIGHT CONSOLIDATION

Gibson *et al.* (1981) derived the following governing equation for finite-strain one-dimensional consolidation of a saturated clay layer using continuity condition, mass conservation, momentum balance and Darcy's law:

$$-\frac{\partial e}{\partial t}=\frac{\partial}{\partial z}\left[\frac{k}{(1+e)\gamma_w}\frac{d\sigma'}{de}\frac{\partial e}{\partial z}\right]+\frac{\partial}{\partial e}\left[\left(\frac{k}{1+e}\right)\left(\frac{\gamma_s-\gamma_w}{\gamma_w}\right)\right]\frac{\partial e}{\partial z} \quad (1)$$

where z is the vertical material coordinate measured upwards, t is time, k is the vertical permeability of the soil, e is the void ratio, σ' is the vertical effective stress, and γ_s and γ_w are the unit weights of soil and water respectively. Note that the material coordinate z is related to the Lagrangian coordinate (a) as $z = \int_0^a \frac{1}{1+e_0(a)}da$, where e_0 is the void ratio at time $t = 0$. The material coordinate z is independent of time, and represents the thickness of the soil particles lying between the datum plane and the point being analysed.

Because of the complex form of the above equation, Gibson *et al.* (1981) provided the solution of its linearised form by assuming the following two functions (g and λ) to be constant.

$$g=-\frac{k}{\gamma_w(1+e)}\frac{d\sigma'}{de} \quad (2)$$

and

$$\lambda=-\frac{d}{de}\left(\frac{de}{d\sigma'}\right) \quad (3)$$

Subsequent studies, however, have shown that the functions $g(e)$ and $\lambda(e)$ are highly variable for most clays, and that the use of constant values for these two functions would result in poor predictions (Benson & Sill, 1985; Carrier, 1985; Govindaraju *et al.*, 1999). This has led to a number of proposals for their variation using simple empirical equations, especially based on power functions. A summary of these relations is presented in Table 1.

PROPOSED STATE-DEPENDENT CONSTITUTIVE RELATIONSHIP FOR SOFT SOILS

Sills (1995, 1998) examined the self-weight consolidation behaviour of sediments using a number of well-controlled settling column test results. One of the unique features of these tests is the non-destructive measurement of the density distribution of solids during the progress of self-weight consolidation, using X-rays. Fig. 2 shows the changes in void ratio with effective stress of three settling column tests (DME10, DME11, and KB8) conducted on Combwich mud, a natural silty clay (LL = 63% and PL = 30%). The base of the settling column was undrained, and therefore drainage occurred only at the top. Other details of these tests are presented in Sills (1995, 1998) and Elder (1985).

The data points in Figs 2(a)–2(c) correspond to the e–σ' path followed by a specific soil horizon, as represented by the dimensionless material coordinate η. The coordinate η is a measure of the fraction of particles that are above a given horizon. For example, $\eta = 0{\cdot}2$ indicates that 20% of the soil particles remain above that level. It is evident from these figures that the e–σ' paths followed by the soil elements at low stress levels are very much dependent on the state of the element with respect to its location. This pattern of non-unique e–σ' paths is also evident in other settling column tests (Been & Sills, 1981; Sills, 1995, 1998; Bartholomeeusen *et al.*, 2002). This feature, however, is absent in existing compressibility models (Table 1), as they assume that all soil elements follow a unique void ratio–effective stress path (e–σ') regardless of its location within the soil column or on the time required to attain a specific effective stress level.

It is also of interest to note that most of the data points collapse onto a single e–σ' curve beyond a threshold stress, $\sigma'_c \approx 1{\cdot}9$ kPa (Figs 2(a)–2(c)). The presence of a threshold stress beyond which a unique e–σ' is found is also evident from the test results reported on other soils under varying experimental conditions (Sills, 1998; Bartholomeeusen *et al.*, 2002). For example, $\sigma'_c \approx 0{\cdot}8$ kPa is found for the settling column tests of Sidere.

Since the time required to attain the same effective stress through pore water pressure dissipation is different for the soil elements along the depth, Sills (1995) has attributed the difference in the e–σ' paths to be the result of the creep of soil. Toorman (2001) has surmised that the non-uniqueness of the constitutive relationships is the result of structural changes of the original building blocks of the sediment bed, the flocs, which lose their identity as they break up under

Table 1. Constitutive models used for self-weight consolidation analysis

	Compressibility	Permeability	Constants	Sources and users
I	$g = -\frac{k}{\gamma_w(1+e)}\frac{d\sigma'}{de} = \text{constant};\ \lambda = -\frac{d}{de}\left(\frac{de}{d\sigma'}\right) = \text{constant}$		g and λ	Gibson *et al.* (1981)
II	$g = -\frac{k}{\gamma_w(1+e)}\frac{d\sigma'}{de} = \text{constant};\ k = \gamma_w \bar{k}(1+e)$		g and $\bar{k}$	Been & Sills (1981)
III	$e = (e_0 - e_\infty)\exp(-\lambda\sigma') + e_\infty$	$k = k^* \exp(\kappa e)$	λ, κ and k^*	Govindaraju *et al.* (1999)
IV	$e = e^* - C_c \log \sigma'$	$c_v = \text{const.}$	e^*, C_c, C and D	Sills (see Bartholomeeusen *et al.* (2002))
V	$e = C_1 \sigma'^{C_2} - 1$	$k = C_3(1+e)^{C_4}$	C_1–C_4 C_2 is negative	Yamaguchi *et al.* (1991)†
VI	$\sigma' = M\varepsilon^N$	$k = (1+e)(\alpha_2 + \beta_2 e)$	M, N, α_2 and β_2	Monte & Krizek (1976)
VII	$e = A\sigma'^B$	$k = Ce^D$	A, B, C & D B is negative	Somogyi (1979); McVay *et al.* (1986)
VIII	$e = A\sigma'^B$	$k = \frac{Ee^F}{1+e}$	A, B, E and F	Carrier *et al.* (1983)
IX	$e = c_1 \sigma'^{c_2} + c_3$	$k = c_4(1+e)\sigma'^{c_5}$	c_1–c_5 c_2 is negative	Koppula & Morgenstern (1982)†
X	$e = A_1(\sigma' + A_2)^{A_3}$	$k = Ce^D$	A_1–A_3, C and D A_3 is negative	Liu & Znidarčié (1991)
XI	$\sigma' = K_\sigma \phi^{-n}$	$k = K_k \phi^{-n}$	K_σ, K_k and n	Winterwerp (1999); Merckelbach & Kranenburg (2004) proposed similar form using clay and sand fraction
XII	$\phi = \phi_0(1 + c_6\sigma')^{c_7}$	$k = k_0(1 + c_6\sigma')^{-c_8}$	ϕ_0, k_0, c_6–c_8	Diplas & Papanicolau (1997)†
XIII	$\sigma' = \exp(m_1 + m_2 e)$	$k = \exp(m_3 + m_4 e)$	m_1–m_4 m_2 and m_3 are negative	Van Kessel & Van Kesteren (2002)

g = finite strain coefficient of consolidation; e_0 and e_∞ = void ratio at zero and infinite effective stress respectively; ε = vertical strain; $\phi = 1/(1+e)$

† Relationship obtained after some algebraic manipulation from its original form.

the increasing load, partly releasing their previously immobilised interstitial pore water.

We believe that the soil skeleton must be fully developed and able to withstand stress without sudden changes in order for creep to be sustained. The structure of freshly sedimented flocs is quite weak, and any increase in effective stress, hydrodynamic drag or seepage force during consolidation could cause it to break down. Increase in stress first destroys the loose aggregate of flocs and then compresses the flocs themselves. With progress of consolidation, the breakdown of the flocs releases the immobilised interstitial pore water, resulting in a decrease in void ratio. The observation of a threshold stress beyond which all test data follow a unique e–σ' curve gives credence to the belief that beyond this stress no such structural changes occur.

Laboratory test results on self-weight consolidation show that the state (e, σ') of soil elements at the end of pore pressure dissipation can be represented by a unique void ratio effective stress line (Imai, 1981). This line represents the compression line at the end of primary consolidation, and will be defined as the EOPCL here. The void ratio on the EOPCL is defined by e_f. The EOPCL is similar to the sedimentation compression line (SCL; Skempton, 1970) or the intrinsic compression line (ICL; Burland, 1990) for natural clays. However, since void ratio may continue to reduce in natural soils over geological periods after excess pore pressure dissipation, the EOPCL would generally lie above the SCL or ICL in an e–σ' plot.

Since a well-defined soil skeleton is formed at the EOPCL, creep and other phenomena could influence its characteristics during subsequent loading or geological ageing. Such behaviour can be modelled using the concept of structural viscosity of the soil skeleton, as has been done elsewhere (Hawlader *et al.*, 2003). It is recognised that while the proposed mechanism captures the essence of structural breakdown and associated phenomena in carefully controlled settling column tests, the process in the field is complex, and would be affected by other factors such as drainage condition, biochemical effects and rate of filling.

The dependence on the state of the soil elements to reach the EOPCL, e–σ' path during self-weight consolidation is modelled here by

$$e = (e_0 - e_f)\exp\left(-\chi\frac{\sigma' - \sigma'_0}{\bar{u}}\right) + e_f \tag{4}$$

where $\bar{u} = \langle \sigma'_m - \sigma' \rangle$; e_0 and σ'_0 are the initial void ratio and effective stress respectively; e_f is the EOPCL void ratio corresponding to the current effective stress (σ'); and χ is an empirical constant. The Macaulay bracket notation $\langle \cdot \rangle$ indicates $\langle \sigma'_m - \sigma' \rangle = \sigma'_m - \sigma'$ if $(\sigma'_m - \sigma') \geqslant 0$ and $\langle \sigma'_m - \sigma' \rangle = 0$ if $(\sigma'_m - \sigma') < 0$. The determination of the stress σ'_m is explained later. Moreover, $\bar{u}$ is a form of pore pressure at low stress level. We note that Sills (1995) had previously recognised the need for normalising the self-weight consolidation test data with some form of excess pore pressure to account for the anomalous behaviour at low effective stress level.

Back-analysis of past test results (Sills, 1995, 1998) has shown that χ varies between 1·5 and 2·5. Note that for large values of χ all soil elements essentially follow the unique void ratio–effective stress path, as used in the current models (Table 1).

In order to examine the physical significance of equation (4), consider a soil element above which the thickness of solid particles is z'. The thickness z' is related to the

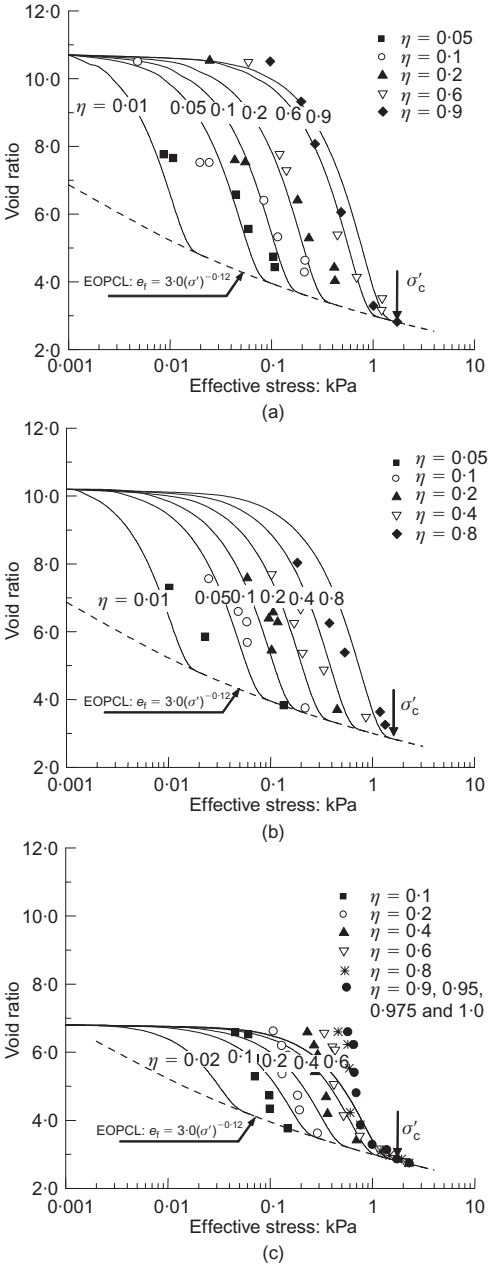

Fig. 2. e–log σ' path followed by soil element during progress of consolidation (solid lines, present model; data points, Sills, 1995): (a) test DME10; (b) test DME11; (c) test KB8

material coordinate system through $z' = h - z$, where h is the total thickness of solid particles in the consolidating soil layer. After the end of excess pore water pressure dissipation, the effective stress at this level is $(\gamma_s - \gamma_w)z'$. The value of σ'_m in equation (4) is equal to $(\gamma_s - \gamma_w)z'$ if $\sigma'_c \geqslant (\gamma_s - \gamma_w)z'$; otherwise $\sigma'_m = \sigma'_c$. This ensures that those soil elements that attain an effective stress larger than σ'_c at the end of pore pressure dissipation will essentially follow the same e–σ' path. This had indeed been observed in past laboratory tests: for example, Fig. 2(c) shows that e–σ' paths for $\eta = 0{\cdot}8$ to $1{\cdot}0$ were nearly identical.

The proposed model suggests that it is necessary to determine the EOPCL and two additional model parameters (σ'_c and χ) to better describe the compression behaviour of soft sediments. Note that for small values of σ'_c the void ratio–effective stress path would become essentially the same as used in current models (Table 1), irrespective of the location of the element in the soil layer.

END OF PRIMARY CONSOLIDATION LINE (EOPCL)

Reliable determination of the consolidation characteristics of soft sediments at low effective stress levels is quite difficult, and conventional oedometer tests cannot be used. Settling column or slurry consolidometer tests have been used in the past for this purpose. However, these tests are quite time consuming (Carrier *et al.*, 1983; Sills, 1995).

Imai (1979) had developed a 'hydraulic consolidation test' device for measuring consolidation characteristics of sediments at low effective stresses. In this test, a downward seepage force is imposed by creating a hydraulic head difference across the specimen, resulting in the consolidation of the soil specimen. After steady flow conditions are attained, the pore pressure is measured, and the void ratio distribution along the length of the specimen is determined by slicing. Using these data, the e–σ' relationship can be developed, which in effect represents the EOPCL, because the change in void ratio due to excess pore pressure dissipation is zero at the steady-state condition. It was further found that the e–σ' line at the end of pore water pressure dissipation in settling column tests was very close to that obtained from the hydraulic consolidation test (Hawlader, 1998). Therefore the hydraulic consolidation test, which is much quicker than settling column tests, can be used to determine the EOPCL of a sediment layer. Such test results have shown that the EOPCL could be defined by a power functional relationship, $e_f = A\sigma'^B$.

It is noted that both compressibility and hydraulic conductivity relationships are equally important in the prediction of self-weight consolidation. However, the present study has focused on soil compressibility. Based on previous studies, the variation of permeability with void ratio is described using a power function ($k = Ce^D$) in the subsequent analyses.

COMPARISON BETWEEN PREDICTED AND MEASURED e–σ' PATHS

The proposed model is first used to predict the measured e–σ' paths of three settling column test results in Figs 2(a)–2(c) before it is implemented in the numerical model to predict the features of self-weight consolidation. The initial densities of the slurry in tests DME10, DME11 and KB8 were 1147, 1153 and 1220 kg/m^3 respectively, corresponding to initial void ratios of 10·7, 10·2 and 6·8. Note that the initial density of all three experiments is above the structural density of about 1142 kg/m^3 that represents the existence of effective stress from the beginning of the experiment (Sills, 1995). The dashed lines in Figs 2(a)–2(c) represent the EOPCL of the soil layers. By drawing a best-fit line through all of the end data points the EOPCL for these tests is determined to be $e_f = 3{\cdot}0(\sigma')^{-0{\cdot}12}$, where σ' is in kPa. We note that past experimental results have shown the characteristics of the EOPCL to be a function of the initial density, with higher values corresponding to flatter lines (Imai, 1981). The same EOPCL is used here, since the initial density is not significantly different among the three experiments. Other soil parameters used in simulation are $\sigma'_c = 1{\cdot}9$ kPa and $\chi = 2{\cdot}0$. The solid lines in Figs 2(a)–2(c) are the predicted e–σ' paths using the present model, which show that the proposed model captures the state-dependent compression behaviour well.

NUMERICAL IMPLEMENTATION

The governing equation (1) can be written in terms of the effective stress as

$$-\frac{\partial e}{\partial t}=\frac{\partial}{\partial z}\left\{\frac{k}{(1+e)\gamma_{\mathrm{w}}}\left[\frac{\partial \sigma'}{\partial z}+(\gamma_{\mathrm{s}}-\gamma_{\mathrm{w}})\right]\right\} \tag{5}$$

Defining $A_1=-\partial e/\partial\sigma'$ and $\alpha=k/(1+e)\gamma_{\mathrm{w}}$, the above equation can be rewritten as

$$A_1\frac{\partial \sigma'}{\partial t}=\alpha\frac{\partial^2\sigma'}{\partial z^2}+\left[\frac{\partial \sigma'}{\partial z}+(\gamma_{\mathrm{s}}-\gamma_{\mathrm{w}})\right]\frac{\partial \alpha}{\partial z} \tag{6}$$

The compressibility A_1 can be obtained by replacing $e_{\mathrm{f}}=A\sigma'^{B}$ in equation (4) and differentiating with respect to σ' to give

$$\begin{aligned}A_1=&\left[\chi\Pi\left(e_0-A\sigma'^{B}\right)+AB\sigma'^{B-1}\right]\\&\exp\left(-\chi\frac{\sigma'-\sigma'_0}{\bar{u}}\right)-AB\sigma'^{B-1}\end{aligned} \tag{7}$$

where

$$\Pi=\begin{cases}\dfrac{\sigma'_{\mathrm{m}}-\sigma'_0}{(\sigma'_{\mathrm{m}}-\sigma')^2} & \text{if } (\sigma'_{\mathrm{m}}-\sigma')>0\\ 0 & \text{if } (\sigma'_{\mathrm{m}}-\sigma')\leqslant 0\end{cases}$$

Using $k=Ce^{D}$ it can be shown that

$$\frac{\partial\alpha}{\partial z}=\alpha\beta \tag{8}$$

where

$$\beta=\left[\frac{D}{e}-\frac{1}{(1+e)}\right]\frac{\partial e}{\partial z} \tag{9}$$

Substituting $\partial\alpha/\partial z$ in equation (6) results in

$$\frac{\partial \sigma'}{\partial t}=\frac{\alpha}{A_1}\left\{\frac{\partial^2\sigma'}{\partial z^2}+\beta\left[\frac{\partial \sigma'}{\partial z}+(\gamma_{\mathrm{s}}-\gamma_{\mathrm{w}})\right]\right\} \tag{10}$$

The governing equation under a given boundary condition was solved numerically using Crank–Nicolson's finite difference technique (Thomas, 1995).

The vertical position of the grid point in the consolidation soil layer is denoted by the subscript n (inset of Fig. 3), and the superscript k is used for time. For a grid point (n,k), equation (10) can be written according to Crank–Nicolson's scheme as

$$\frac{\sigma'^{\,k+1}_n-\sigma'^{\,k}_n}{\Delta t}=\frac{1}{2}\left[\Lambda\left(\sigma'^{\,k+1}_n\right)+\Lambda\left(\sigma'^{\,k}_n\right)\right] \tag{11}$$

where $\sigma'^{\,k}_n$ and $\sigma'^{\,k+1}_n$ are the discrete solutions of equation (10), and $\Lambda(\sigma'^{\,k}_n)$ and $\Lambda(\sigma'^{\,k+1}_n)$ are the discrete difference operators at time steps k and $k+1$ respectively.

Use of central finite difference approximation on equation (10) results in

$$\Lambda\left(\sigma'^{\,k}_n\right)=P\sigma'^{\,k}_{n+1}+Q\sigma'^{\,k}_n+R\sigma'^{\,k}_{n-1}+S \tag{12}$$

in which

$$\begin{aligned}P&=\frac{\alpha}{A_1(z_{n+1}-z_{n-1})}\left(\frac{2}{z_{n+1}-z_n}+\beta\right)\\ Q&=-\frac{2\alpha}{A_1(z_{n+1}-z_{n-1})}\left(\frac{1}{z_{n+1}-z_n}+\frac{1}{z_n-z_{n-1}}\right)\\ R&=\frac{\alpha}{A_1(z_{n+1}-z_{n-1})}\left(\frac{2}{z_n-z_{n-1}}-\beta\right)\\ S&=\frac{(\gamma_{\mathrm{s}}-\gamma_{\mathrm{w}})\alpha\beta}{A_1}\end{aligned} \tag{13}$$

A similar expression can be written for $\Lambda(\sigma'^{\,k+1}_n)$. Now, substitution of the expressions $\Lambda(\sigma'^{\,k}_n)$ and $\Lambda(\sigma'^{\,k+1}_n)$ into equation (11) leads to a tridiagonal matrix system of equations for the new values of $\sigma'^{\,k+1}_{n-1}$, $\sigma'^{\,k+1}_n$ and $\sigma'^{\,k+1}_{n+1}$ as

$$C_{1,n}\sigma'^{\,k+1}_{n-1}+C_{2,n}\sigma'^{\,k+1}_n+C_{3,n}\sigma'^{\,k+1}_{n+1}=C_{4,n} \tag{14}$$

where

$$\begin{aligned}C_{1,n}&=-P\Delta t/2\\ C_{2,n}&=1-Q\Delta t/2\\ C_{3,n}&=-R\Delta t/2\\ C_{4,n}&=\sigma'^{\,k}_n+\left(P\sigma'^{\,k}_{n+1}+Q\sigma'^{\,k}_n+R\sigma'^{\,k}_{n-1}+2S\right)\Delta t/2\end{aligned} \tag{15}$$

The constants $C_{i,n}$ ($i=1, 2, 3, 4$) in equation (15) are calculated at the grid points along z ($n=2, 3, 4, \ldots, L-1$) during computation (inset of Fig. 3). Incorporating the boundary conditions for the first and last nodes (i.e. nodes 1 and L), the simultaneous equations (14) for different nodes are solved to obtain $\sigma'^{\,k+1}$. An efficient solution procedure has been developed for this diagonally dominant tridiagonal matrix system using LU decomposition and forward- and back-substitution. Once the value of σ' for the time step $k+1$ is known, the void ratio is calculated for this time step. By updating the values of α, β and A_1 based on the average values of e $(=(e^k_n+e^{k+1}_n)/2)$ and σ' $(=(\sigma'^{\,k}_n+\sigma'^{\,k+1}_n)/2)$, the calculation is repeated for this time step until the difference between two successive iterations is less than 10^{-10}. The computation then shifts to the next time step and the process is repeated.

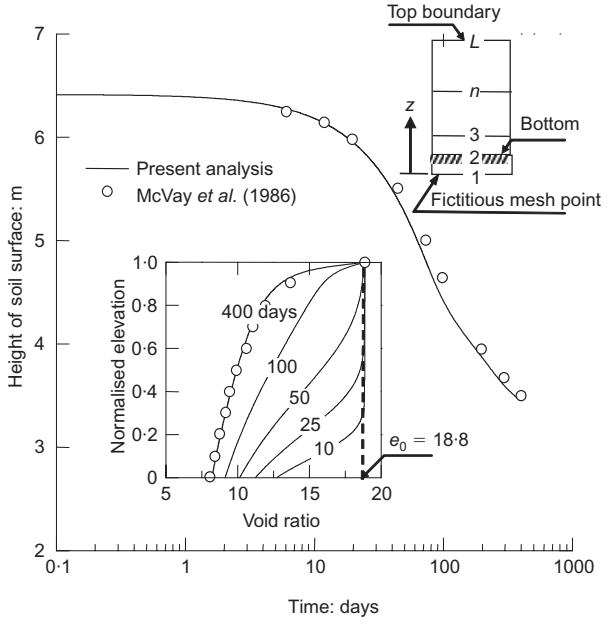

Fig. 3. Verification of numerical analysis

INITIAL AND BOUNDARY CONDITIONS

Initial condition

The progress of consolidation is assumed to start from a constant initial void ratio (e_0). If the initial density of slurry (ρ_0) is more than the structural density (ρ_{s}), the soil structure exists from the beginning of the test. The value of e_0 can be calculated by $(G_{\mathrm{s}}-1)\rho_{\mathrm{w}}/(\rho_0-\rho_{\mathrm{w}})-1$, where G_{s} is the specific gravity of soil particles and ρ_{w} is the density of water. However, if ρ_0 is less than ρ_{s} then e_0 is the void ratio at which sedimentation ceases, and consolidation is assumed to start in the sedimented soil bed. The value of e_0

corresponds to the structural density (Sills, 1995), which is also similar to the fluid limit (Monte & Krizek, 1976). Previous studies have shown that the water content at the beginning of consolidation is about five to seven times the liquid limit (Monte & Krizek, 1976; Carrier *et al.*, 1983). Stark *et al.* (2005) have observed a correlation between e_0 and plasticity index (PI) as $e_0 = 8{\cdot}25 + 0{\cdot}02\text{PI}$ for inorganic clays of high plasticity. Further information on selecting e_0 is available in Carrier *et al.* (1983) and Stark *et al.* (2005).

Boundary conditions

The effective stress at the top of the soil layer remains zero always (i.e. $\sigma'_L = 0$). An impermeable boundary condition needs to be used where the sedimented soil overlies an impervious and incompressible layer. A fictitious node point (node 1 in the inset to Fig. 3) below the bottom boundary of the soil layer is used to define this condition. The flow velocity through the undrained surface is zero throughout the progress of consolidation. Thus

$$\frac{\partial \sigma'}{\partial z} = -(\gamma_s - \gamma_w) \tag{16}$$

Using finite difference approximation the above can be rewritten as

$$\sigma'_1 = \sigma'_2 + (z_2 - z_1)(\gamma_s - \gamma_w) \tag{17}$$

It is noted that the rate of consolidation is high at the beginning of the test. Therefore the initial time step in the calculation has been kept small enough to achieve an accurate solution. In this study, the initial time step of 1 s is used, and it is advanced according to $\Delta t^k = 1{\cdot}005 \times \Delta t^{k-1}$.

VERIFICATION OF NUMERICAL ANALYSIS

In order to check the accuracy of the space–time discretisation of the highly non-linear consolidation process, the numerical code is compared with previous predictions of the self-weight consolidation of a phosphatic clay layer having the initial void ratio of 18·8 by McVay *et al.* (1986). The initial height of the clay layer is 6·33 m and the base is undrained. The compressibility and hydraulic conductivity are modelled using $e = 12{\cdot}2(\sigma')^{-0{\cdot}29}$ and $k = 1{\cdot}4 \times 10^{-11} e^{4{\cdot}11}$, where σ' and k are in kPa and m/s respectively (McVay *et al.*, 1986). Note that the e–σ' relationship in this case is different from the present study (equation (4)), and therefore in the computer program the compressibility $A_1 = -\mathrm{d}e/\mathrm{d}\sigma' = 3{\cdot}54(\sigma')^{-1{\cdot}29}$ has been used for this case instead of equation (7). The predicted height of the soil layer with the progress of consolidation is identical to those by McVay *et al.* (1986), as shown in Fig. 3. The inset of Fig. 3 shows the change in void ratio with normalised depth. The predicted void ratio profile after 400 days of consolidation also matches well with McVay *et al.* (1986). These results confirm the validity of the present finite difference discretisation and numerical algorithms.

SIMULATION OF SIDERE TEST RESULTS

The initial conditions of the Sidere experiments are shown in the inset of Fig. 4. Experiments Sidc2, Sidc3, Sidc5 and Sidc6 were the calibration experiments, and Sidp1 was the prediction experiment. The initial heights (h_0) of the experiments were 0·2–0·6 m. As shown in the figure inset, all experiments started with reasonably close initial densities (ρ_0), except experiment Sidc5, which started with a lower density. However, the initial densities of all experiments are greater than the structural density that ensured commencement of self-weight consolidation from the very beginning. Note that these densities are also higher than those reported in Figs 2(a)–2(c). By drawing a best-fit line through all of the lowest data points the EOPCL for these tests is determined to be $e_f = 1{\cdot}43(\sigma')^{-0{\cdot}064}$, where σ' is in kPa. The variation of permeability for these experiments is defined by the power function $k = 6 \times 10^{-9} e^{6{\cdot}6}$ m/s. In addition, the model parameters $\sigma'_c = 0{\cdot}8$ kPa and $\chi = 2{\cdot}0$ are used. It can be seen that the prediction of the model captures the progress of consolidation in the experiments and the surface settlement profile quite well (Fig. 4).

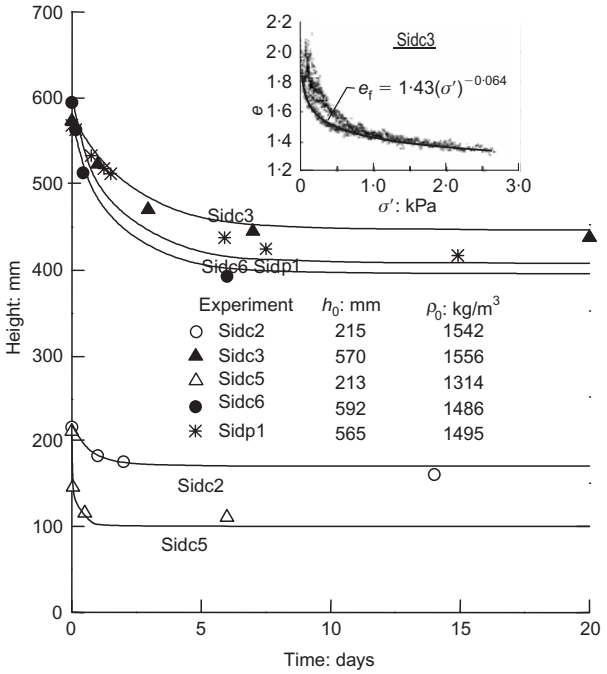

Fig. 4. Comparison between experimental and predicted surface settlement (solid lines, present model; data points, Bartholomeeusen *et al.*, 2002)

The experiment Sidc3 is selected for further analyses to elicit some of the salient features of the proposed model. Fig. 5 shows the predicted void ratio–effective stress path followed by the various soil elements. It is evident that their e–σ' paths are different for stress levels less than σ'_c. By plotting the effective stress on a natural scale, the void ratio–effective stress relationship is compared with experimental data points, as shown in Fig. 5(b). The predicted e–σ' path agrees very well with experimental observations. The dashed lines in Fig. 5(a) represent the progress of consolidation for selected days. Similar types of consolidation time line have also been reported from settling column test results (Sills, 1995). The use of a single e–σ' curve, as in the current practice, cannot simulate this important behaviour at low stress levels.

The surface settlement profile is important for designing storage volume of dredged material, but the density profile and pore pressure dissipation are of main interest for developing erosion resistance of a river bed and resuspension of mine tailings due to dynamic loading under water cover, because the strength of a sedimented soil bed depends on the effective stress and void ratio. Thus successful modelling of the self-weight consolidation process must include not only the surface settlement but also prediction of the void ratio profile. Fig. 6 shows the predicted and measured excess pore water pressure at different time periods. The top of the curves represents the height of the soil layer, which gradually decreases, as shown in Fig. 4. Consolidation begins with a linear variation of excess pore pressure at zero days having

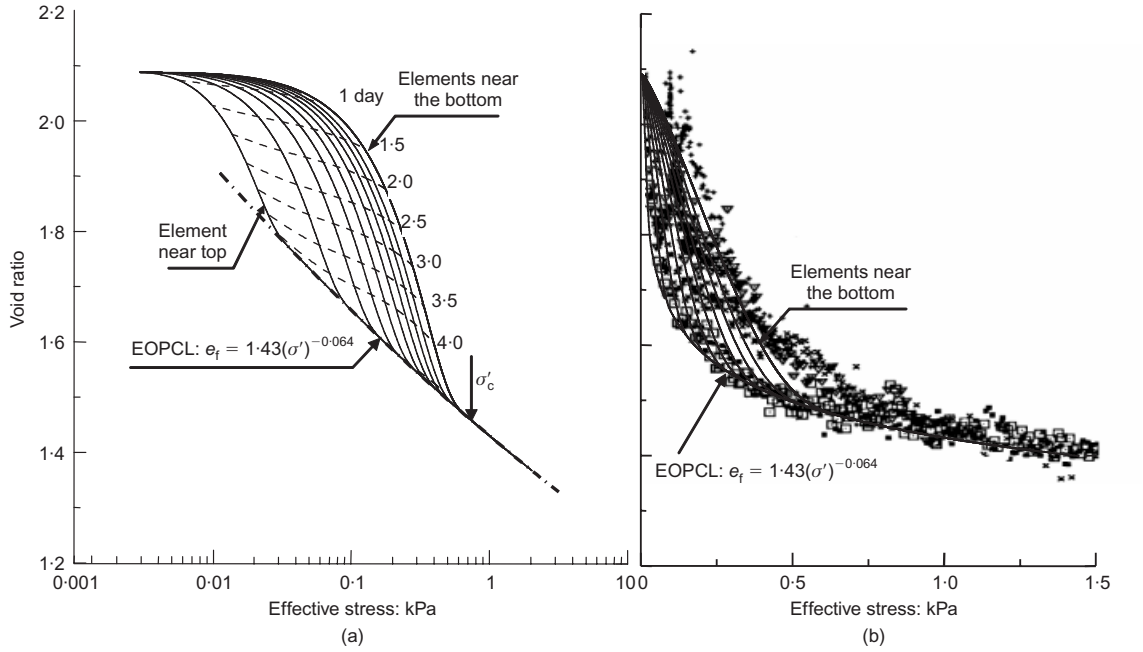

Fig. 5. e–σ' path followed by soil elements, test Sidc3 (solid lines, present model; dashed lines, consolidation time lines; data points, Bartholomeeusen *et al.*, 2002) : (a) logarithmic scale ; (b) natural scale

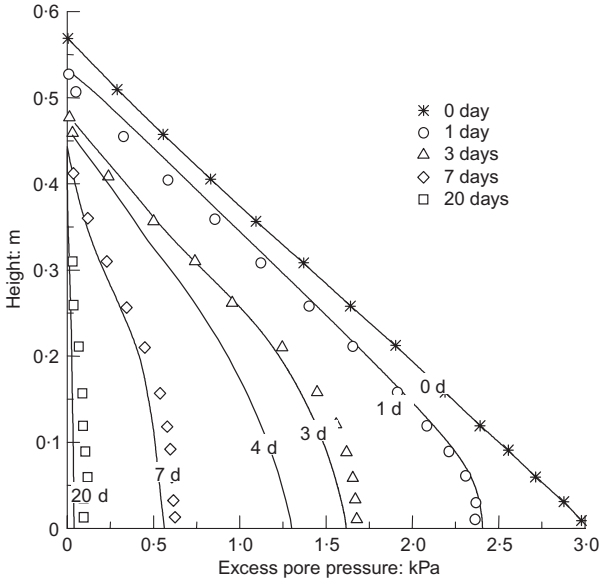

Fig. 6. Predicted and measured excess pore water pressure, test Sidc3 (Bartholomeeusen *et al.*, 2002)

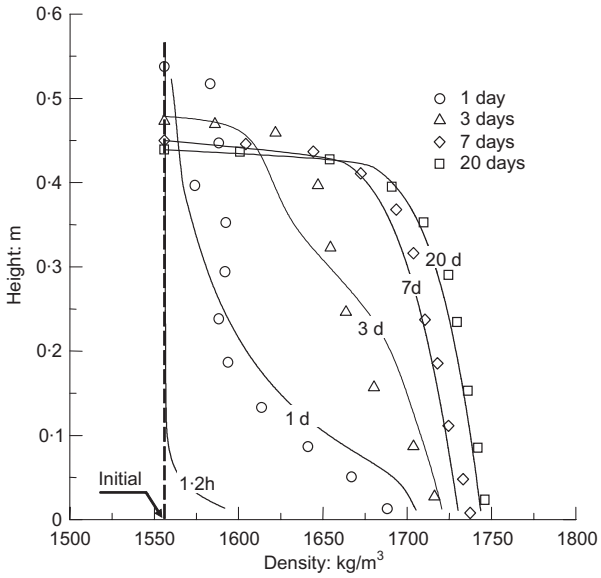

Fig. 7. Predicted and measured density profiles, test Sidc3 (Bartholomeeusen *et al.*, 2002)

slope of $(\gamma_s - \gamma_w)/(1 + e_0)$. The pore water pressure is almost completely dissipated at the end of 20 days. Fig. 7 shows the comparison between measured and predicted density profile with the progress of consolidation. These figures show that the present model can well simulate excess pore pressure and void ratio profiles.

The solid lines in Fig. 8 show the change in void ratio of soil elements for given effective stresses (0·05–2·3 kPa). Note that the start of the line represents the time at which a soil element first reaches the given stress level. Since consolidation starts from the bottom of the soil layer, the elements near the bottom attain an effective stress earlier than those near the top. It can be seen that the predicted void ratio for a given effective stress is not constant, but decreases with time for effective stresses less than σ'_c. The figure also shows measured data points at four effective stresses (0·1, 0·4, 1·2 and 2·3 kPa). The numerical prediction agrees very well with measured values. The dashed lines in this figure show the predicted values using a unique power function compressibility model ($e = A\sigma'^B$). It can be seen that it leads to a constant void ratio for a given effective stress, and thus cannot capture the decreasing void ratio pattern with time at low stress levels. Use of any other unique e–σ' compressibility law (Table 1) would suffer the same deficiency in this respect. It is noted, however, that at higher stress levels ($\sigma' \geqslant \sigma'_c$) both types of model yield similar results. This means that at higher stresses the void ratio is constant, irrespective of the location for a given effective stress level, as observed in laboratory tests (e.g. at $\sigma' = 1{\cdot}2$ and 2·3 kPa in Fig. 8).

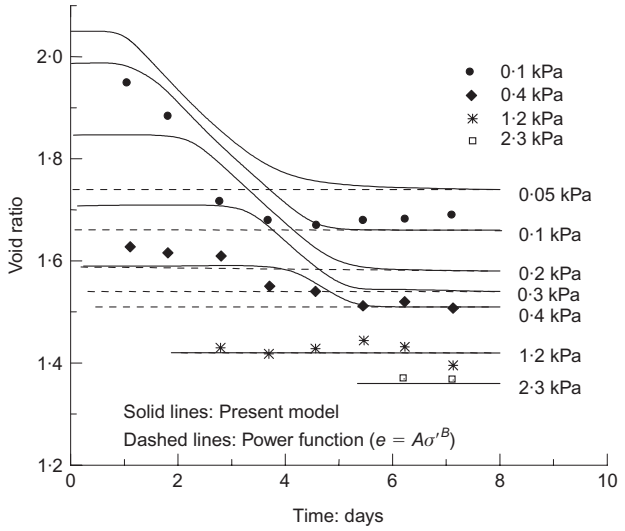

Fig. 8. Predicted and measured void ratio at constant effective stress levels, test Sidc3: solid lines, present model; dashed lines, power function, $e = A\sigma'^{B}$ (data points, Bartholomeeusen *et al.*, 2002)

DISCUSSION AND CONCLUSIONS

The process of the development of structure in soils resulting from sedimentation and self-weight consolidation is complex. Structural changes of the flocs occur as they break up under increasing loads, partly releasing their previously immobilised interstitial pore water, resulting in non-uniqueness of constitutive relationships. This is evident from a closer examination of self-weight consolidation behaviour in settling column tests, which show that at low effective stress levels the compressibility behaviour of soil elements is very much dependent on their location. Failure to account for this non-uniqueness in compressibility in current models has resulted in poor predictions at the early stages of consolidation. The observation of a threshold stress beyond which all test data follow a unique e–σ' curve suggests that beyond this stress (σ'_c) no such structural changes occur, and a unique compressibility behaviour exists. A new compressibility model that recognises these facts is developed.

The model requires the void ratio–effective stress relationship at the end of primary consolidation (EOPCL), the threshold stress (σ'_c) and a soil constant (χ) to better describe the compression behaviour of soft sediments. The type of soil, salt concentration and initial density influence the choice of the model parameters. The characteristics of the EOPCL are dependent on initial density, and higher density would result in a flatter line. The value of χ lies between 1·5 and 2·5, although the use of $\chi = 2{\cdot}0$ is able to simulate the overall trend of the experimental results reasonably well. It is, however, noted that lower values of χ were found to better capture the measured e–σ' points of experiments that started with higher initial density (e.g. KB8 and Sidc3).

The governing differential equation for consolidation is discretised by employing the Crank–Nicolson finite difference scheme. It was solved using the new constitutive model and appropriate initial and boundary conditions. Comparisons between predicted and experimental results show that the proposed model can successfully simulate the settlement of soil layer, void ratio and pore water pressure distributions with the progress of consolidation. More importantly, the non-unique void ratio of soil elements at a given effective stress, as observed in laboratory experiments, can be simulated using the proposed model.

NOTATION

a	Lagrangian coordinate
c_v	coefficient of consolidation
EOPCL	end of primary consolidation line
e	void ratio
e_0	initial void ratio
e_f	void ratio at EOPCL
G_s	specific gravity of soil solids
h	height of soil solids
k	vertical permeability
t	time
Δt	time increment
$\bar{u}$	a form of pore water pressure
z	material coordinate
ε	vertical strain
η	dimensionless material coordinate
ϕ	solids volume fraction
γ_s	unit weight of soil solids
γ_w	unit weight of water
χ	empirical constant
ρ_0	initial density of slurry
ρ_s	structural density of slurry
ρ_w	density of water
σ'	effective stress
σ'_0	initial effective stress
σ'_c	threshold stress

REFERENCES

Bartholomeeusen, G., Sills, G. C., Znidarčić, D., Van Kesteren, W., Merckelbach, L. M., Pyke, R., Carrier, W. D. III, Lin, H., Penumadu, D., Winterwerp, H., Masala, S. & Chan, D. (2002). Sidere: numerical prediction of large-strain consolidation. *Géotechnique* **52**, No. 9, 639–648.

Been, K. & Sills, G. C. (1981). Self-weight consolidation of soft soils. *Géotechnique* **31**, No. 4, 519–535.

Benson, R. E. Jr & Sill, B. L. (1985). Discussion of 'Prediction of consolidation of very soft soil' by K. W. Cargill. *ASCE J. Geotech. Engng* **111**, No. 11, 1356–1358.

Burland, J. B. (1990). On the compressibility and shear strength of natural clays. *Géotechnique* **40**, No. 3, 329–378.

Carrier, W. D. III (1985). Discussion of 'Prediction of consolidation of very soft soil,' by K. W. Cargill. *J. Geotech. Engng.* **111**, No. 11, 1358–1360.

Carrier, W. D. III, Bromwel, L. G. & Somogyi, F. (1983). Design capacity of slurried mineral waste ponds. *ASCE J. Geotech. Engng* **109**, No. 5, 699–716.

Diplas, P. & Papanicolaou, A. (1997). Batch analysis of slurries in zone settling regime. *ASCE J. Environ. Engng* **123**, No. 7, 659–667.

Elder, D. McG. (1985). *Stress–strain and strength behaviour of very soft soil sediment*. DPhil thesis, University of Oxford, UK.

Gibson, R. E., Schiffman, R. L. & Cargill, K. W. (1981). The theory of one-dimensional consolidation of saturated clays. II. Finite nonlinear consolidation of thick homogeneous layers. *Can. Geotech. J.* **18**, No. 2, 280–293.

Govindaraju, R. S., Ramireddygari, S. R., Shrestha, P. L. & Roig, L. C. (1999). Continuum bed model for estuarine sediments based on nonlinear consolidation theory. *ASCE J. Hydraul. Engng* **125**, No. 3, 300–304.

Hawlader, B. C. (1998). *Elasto-viscoplastic analysis of one-dimensional consolidation of soft clay.* PhD thesis, Yokohama National University, Japan.

Hawlader, B. C., Muhunthan, B. & Imai, G. (2003). Viscosity effects on one-dimensional consolidation of clay. *ASCE Int. J. Geomech.* **3**, No. 1, 99–110.

Imai, G. (1979). Development of a new consolidation test procedure using seepage force. *Soils Found.* **19**, No. 3, 45–59.

Imai, G. (1981). Experimental studies on sedimentation mechanism and sediment formation of clay materials. *Soils Found.* **21**, No. 1, 7–20.

Koppula, S. D. & Morgenstern, N. R. (1982). On the consolidation of sedimenting clays. *Can. Geotech. J.* **19**, No. 3, 260–268.

Liu, J. C. & Znidarčić, D. (1991). Modeling one-dimensional compression characteristics of soils. *ASCE J. Geotech. Engng* **117**, No. 1, 162–169.

McVay, M., Townsend, F. & Bloomquist, D. (1986). Quiescent consolidation of phosphatic waste clays. *ASCE J. Geotech. Engng* **112**, No. 11, 1033–1049.

Merckelbach, L. M. & Kranenburg, C. (2004). Equations for effective stress and permeability of soft mud-sand mixtures. *Géotechnique* **54**, No. 4, 235–243.

Monte, J. L. & Krizek, R. J. (1976). One-dimensional mathematical model for large-strain consolidation. *Géotechnique* **26**, No. 3, 495–510.

Sills, G. C. (1995). Time dependent processes in soil consolidation. *Proceedings of the international symposium on compression and consolidation of clayey soils*, IS-Hiroshima '95, (eds H. Yoshikuni and O. Kusakabe), pp. 875–890. Rotterdam: A. A. Balkema.

Sills, G. C. (1998). Development of structure in sedimenting soils. *Phil. Trans. R. Soc. Lond. A* **356**, 2515–2534.

Skempton, A. W. (1970). The consolidation of clays by gravitational compaction. *Q. J. Geol. Soc.* **125**, 373–412.

Somogyi, F. (1979). *Analysis and prediction of phosphatic clay consolidation: Implementation package*. Technical Report, Florida Phosphatic Clay Research Project, Lakeland, FL.

Stark, T. D., Choi, H. & Schroeder, P. R. (2005). Settlement of dredged and contaminated material placement areas. II: Primary consolidation, secondary compression, and desiccation of dredged fill input parameters. *J. Waterw. Port Coastal Ocean Engng* **131**, No. 2, 52–61.

Thomas, J. W. (1995). *Numerical partial differential equations*: *Finite difference methods.* New York: Springer.

Toorman, E. A. (1996). Sedimentation and self-weight consolidation: general unifying theory. *Géotechnique* **46**, No. 1, 103–113.

Toorman, E. A. (2001). Cohesive sediment transport modeling: European perspective. In *Proc. Marine Science*, Vol. 3: *Coastal and Estuarine Fine Sediment Processes* (eds W. H. McAnally and A. J. Mehta), pp. 1–18. Amsterdam: Elsevier Science.

Van Kessel, T. & Van Kesteren, W. G. M. (2002). Gas production and transport in artificial sludge depots. *Waste Management* **22**, No. 1, 19–28.

Winterwerp, J. C. (1999). *On the dynamics of high-concentrated mud suspensions*. PhD thesis, Delft University of Technology.

Yamaguchi, H., Imai, G., Watanabe, K. & Ogata, K. (1991). Sedimentation consolid. *Proc. Int. Conf. Geotech. Engng. Coastal Development, Geo-Coast 91*, *Yokohama* **1**, 129–134.